Peer-reviewed version available at *Universe* **2019**, *5*, 34; doi:10.3390/universe5010034

Article

Muon Radiography of Ancient Mines: the San Silvestro Archaeo-Mining Park (Campiglia Marittima, Tuscany)

Guglielmo Baccani [1,2]*, Lorenzo Bonechi [2,1], Massimo Bongi [1,2], Debora Brocchini [3], Nicola Casagli [4], Roberto Ciaranfi [2], Luigi Cimmino [5,6], Vitaliano Ciulli [1,2], Raffaello D'Alessandro [1,2], Chiara Del Ventisette [4], Andrea Dini [7], Giovanni Gigli [4], Sandro Gonzi [1,2], Silvia Guideri [3], Luca Lombardi [4], Barbara Melon [2], Massimiliano Nocentini [4], Pasquale Noli [5,6], Nicola Mori [2,1], Giulio Saracino [5,6] and Lorenzo Viliani [2,1]

1 Università di Firenze, Dipartimento di Fisica e Astronomia, Via G. Sansone 1, I-50019 Sesto Fiorentino (Firenze), Italy
2 Istituto Nazionale di Fisica Nucleare, Sezione di Firenze, Via B. Rossi 3, I-50019 Sesto Fiorentino (Firenze), Italy
3 Parchi Val di Corchia S.p.A., via Lerario, 90, 57025 Piombino, Italy
4 Università di Firenze, Dipartimento di Scienze della Terra, Via G. La Pira 4-50121, Firenze, Italy
5 Università degli Studi di Napoli Federico II - Dipartimento di Fisica, Complesso Universitario di Monte Sant'Angelo - Via Cintia, 21 - 80126 - Napoli, Italy
6 Istituto Nazionale di Fisica Nucleare, Sezione di Napoli, Complesso Universitario di Monte Sant'Angelo - Via Cintia, 80126 Napoli, Italy
7 CNR-Istituto di Geoscienze e Georisorse, Pisa, Italy
* Correspondence: guglielmo.baccani@fi.infn.it

Abstract: Muon radiography is an imaging technique based on the measurement of the absorption of cosmic ray muons. This technique has recently been used successfully to investigate the presence of unknown cavities in the Bourbon Gallery in Naples and in the Cheops Pyramid at Cairo. The MIMA detector (Muon Imaging for Mining and Archaeology) is a muon tracker prototype for the application of muon radiography in the Archaeological and Mining fields. It is made of three couples of X-Y planes each consisting of 21 scintillator bars with silicon photomultiplier read-out. The detector is compact, robust, easily transportable and has a low power consumption: all of that makes the detector ideal for measurements in narrow and isolated environments. With this detector we have performed a measurement from inside the Temperino mine in the San Silvestro archaeo-mining park in Tuscany. The park includes about 25 km of mining tunnels arranged on several levels that have been excavated since the Etruscan time. The measured muon absorption was compared to the simulated one, obtained from the information provided by 3D laser scanner measurements and the cartographic maps of the mountain above the mine, in order to obtain information on the average density of the rock. This allowed to confirm the presence of a partially accessible exploitation opening and gave some hints on the presence of a high density body within the rock.

Keywords: muon radiography; cosmic rays; tracking detectors; imaging; geophysical prospection; mining

1. Introduction

When primary cosmic rays enter the atmosphere they produce showers of secondary particles, including mesons like pions and kaons that can decay into muons. For energies greater than 1 GeV muons are the most abundant charged particles in cosmic rays at the sea level: their integrated flux in the vertical direction is about 70 m^{-2} s^{-1} sr^{-1} [1].

Muons are low interacting particles (the most energetic muons in cosmic rays can pass through hundreds of meters in rock) and this allows to use them for radiographical measurements. Muon

radiography is similar to X-rays radiography: it is a non-invasive imaging technique that can be used to measure the mean density of matter along a line of sight. The muon flux measured in different directions is compared to that obtained by simulating the particles propagation through the structure under study reconstructing the two dimensional density profile of the traversed matter.

The muon radiography technique was exploited for the first time in 1955 to determine the rock overburden on a mountain tunnel [2]. In 1970 the Nobel Prize particle physicist Louis Alvarez and his collaborators performed a radiography of the Chefren pyramid in Egypt and they were able to exclude the existence of a hidden burial chamber [3]. After these pioneering measurements recently muon absorption radiography was again taken into consideration, at first by Japanese groups [4] and later by Italian, French, Canadian, American and other groups (e.g. [5–13]), to be applied in the fields of Volcanology, Mining and Archaeology. The MURAVES project (MUon RAdiography of VESuvius) [14], born from the collaboration between INGV (National Institute of Geophysics and Volcanology) and INFN (National Institute of Nuclear Physics), aims at the study of the interior of the Vesuvius volcano near Naples using muon radiography. From the expertise gained in the R&D for the MURAVES experiment is born the MIMA project. Last year a radiography of underground cavities of the Bourbon Gallery at Mt. Echia (Naples) has been made both with Mu-Ray, a prototype for the MURAVES experiment, and MIMA trackers from three different locations confirming the presence of an unknown cavity previously detected by Mu-Ray [9]. Recently a big void in Cheops Pyramid in Cairo has been discovered by the ScanPyramids collaboration using the muography technique [10].

2. The MIMA project

The aim of the MIMA project [15] is to use muon imaging for Archaeological, Mining and Civil Engineering applications, looking for hidden cavities or volumes containing high-density materials. The MIMA tracker is a scaled down replica of the Mu-Ray telescope with different characteristics.

2.1. The detector

MIMA has been designed and built to fulfill a series of requirements among which:

- low power consumption (roughly 30 W) allowing to be powered also by means of a small set of photovoltaic panels;
- lightness and compactness to ease the transportation: MIMA weights almost 60 kg including the mechanics and the tracker is contained into a cubic aluminum frame of 50 cm per side;
- tracking capability with a 14 mrad angular resolution.

The MIMA tracker is composed of three X-Y tracking modules stacked inside a cubic aluminum frame mounted on an altazimuthal platform which allows modifying the telescope pointing direction. A picture of the detector with the three modules clearly visible is reported in Figure 1.a.

Each module consists of two identical and independent tracking planes which in turn are made up of 21 plastic scintillator bars assembled in such a way to produce a 40x40 cm^2 active detection surface. The two planes measure respectively the X and Y coordinates of the muon impact points.

Every bar is readout using two silicon photomultiplier (SiPM) photosensors whose signals are added by a sum card. The read-out system is made of six independent boards, called slave boards, one for each plane, based on the EASIROC chip, a 32 channels analogue front-end ASIC to readout SiPM photosensors. The six slave boards are controlled by a single master board that manages the configuration of the slave boards, the trigger logic and the data file transfer. The control of the acquisition system and the data storage is entrusted to a Raspberry Pi provided of a 64 GB SDHC memory card. The network connection of the Raspberry Pi, although it is not essential, is useful to allow monitoring the status of the instrument.

Preprints (www.preprints.org) | NOT PEER-REVIEWED | Posted: 26 November 2018 doi:10.20944/preprints201811.0595.v1

Peer-reviewed version available at Universe 2019, 5, 34; doi:10.3390/universe5010034

(a) *The tracker* **(b)** *Installation inside the mine*

Figure 1. (**a**) Structure of the MIMA detector: we can see the three X-Y tracking modules, the rotating platform and part of the electronics. (**b**) A picture of the installation inside the Temperino mine. In this case the detector was placed inside a wooden box and it was equipped with an incandescent lamp and two small fans to protect it against moisture.

2.2. Track reconstruction

Muon tracks are reconstructed event by event independently in the X-Z and Y-Z views. Clusters are formed considering one or more neighbouring bars with a signal sufficiently higher than the noise level. In each view a successful alignment (residuals within 2 cm) of clusters belonging to the three planes of the same view defines a candidate projected track. The three-dimensional track is obtained combining the tracks in the two projections. We selected events containing only a single muon track rejecting ambiguous events where more than one track could be reconstructed. For these golden tracks we define an angular acceptance of approximately $\pm 45^\circ$ with respect to the MIMA axis. To increase the acceptance we also included those tracks passing only through the central module and at least one of the outer two. In this case we didn't have the possibility to check the quality of the track but we extended the angular acceptance up to approximately $\pm 60^\circ$.

3. Measurement site and goal

The Park of San Silvestro in Campiglia Marittima is a touristic park, where traces of Etruscan, Medieval and modern mining activity are still visible and partly open to visitors. Mining activity dates back to Etruscan-Roman time ending in 1982. Early miners (Etruscan to medioeval) dug narrow and tortuous shafts following the steeply inclined bodies of skarn (a metasomatic rock made by hedenbergite and ilvaite) rich in Cu-Fe-Pb-Zn-Ag sulfides [16,17]. Locally the concentration of sulfides was exceptional and the excavation resulted in large exploitation openings (up to several hundreds of cubic metres) that were partially backfilled by the subsequent mining activity. Nowadays the Temperino mine is composed of a series of tunnels on multiple levels, with the shallower ones that cut ancient mining shafts.

The aim of our measurement is to test the muon radiography technique in the archaeological and mining fields. Through this method it is possible to detect the presence of cavities and tunnels dug into the rock including the ancient ones, nowadays inaccessible. In particular, we focused on the detection of the signal of a large accessible cavity called Gran Cava (see Figure 2). The Gran Cava is an old, large exploitation opening, directly connected to the surface, that has been enlarged during Renaissance time and modern industrial activity. From the radiography measurement it is also possible to estimate the average density of the rock in various directions along the line of sight of the detector. To do so

Preprints (www.preprints.org) | NOT PEER-REVIEWED | Posted: 26 November 2018 doi:10.20944/preprints201811.0595.v1

Peer-reviewed version available at Universe 2019, 5, 34; doi:10.3390/universe5010034

(a) *Outside view* **(b)** *Inside view*

Figure 2. Pictures of the Gran Cava. (**a**) From the outside view we can see the light from the exit at the end of the cavity where there is a vertical opening. (**b**) In the picture from the inside of the quarry is possible to glimpse us working on the laser scanner survey of the cave.

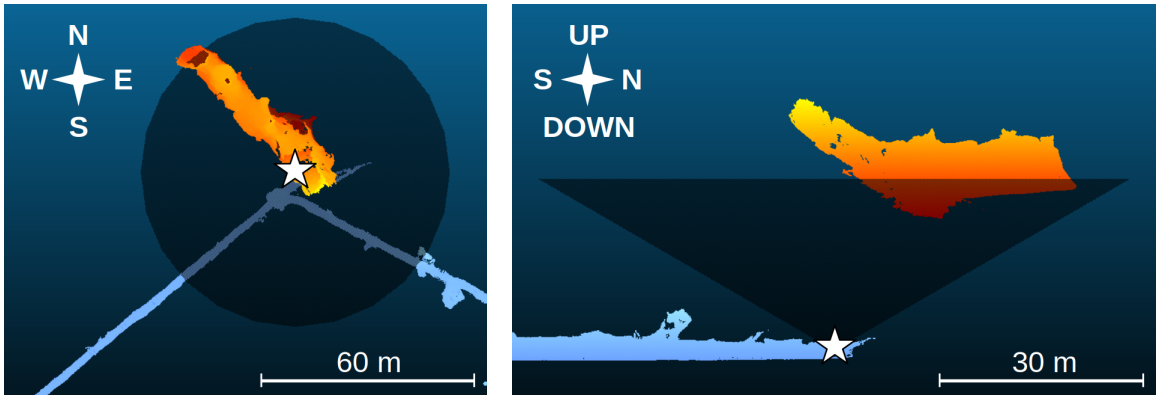

(a) *Top view.* **(b)** *Side view.*

Figure 3. Maps of both the Temperino mine (blue) and the Gran Cava (red). The detector position is indicated with the white star and the acceptance cone ($\pm 60^\circ$ from the vertical direction) is represented with the dark area up to an height of about 25 m. For the sake of clarity the outline of the hill is not reported.

we have made surveys of both the inside of the mine and of the overlying hill through measurements with 3D laser scanner. These surveys were then integrated with a digital terrain model in order to obtain a complete coverage of the area observed by our detector. Maps of both the Temperino mine and the Gran Cava are reported in Figure 3.

For the measurement the tracker was placed in a cave along the tunnel of the Temperino mine just below the Gran Cava and pointed in the vertical direction (Figure 1.b). Approximately $2 \cdot 10^6$ triggers were acquired during 53 days. A free sky calibration sample of about $35 \cdot 10^6$ triggers was acquired on the roof of the building of the Florence section of INFN in 17 days of data taking. From here on we will refer to these two measures respectively as the target (tar) and the free sky configuration (free).

4. Absorption radiography of the Temperino mine

The muon measured transmission T_M as a function of the observing direction (θ, φ) is defined as:

$$T_M(\theta, \varphi) = \frac{\Phi_{M,tar}(\theta, \varphi)}{\Phi_{M,free}(\theta, \varphi)} \quad (1)$$

Preprints (www.preprints.org) | NOT PEER-REVIEWED | Posted: 26 November 2018 doi:10.20944/preprints201811.0595.v1

Peer-reviewed version available at Universe 2019, 5, 34; doi:10.3390/universe5010034

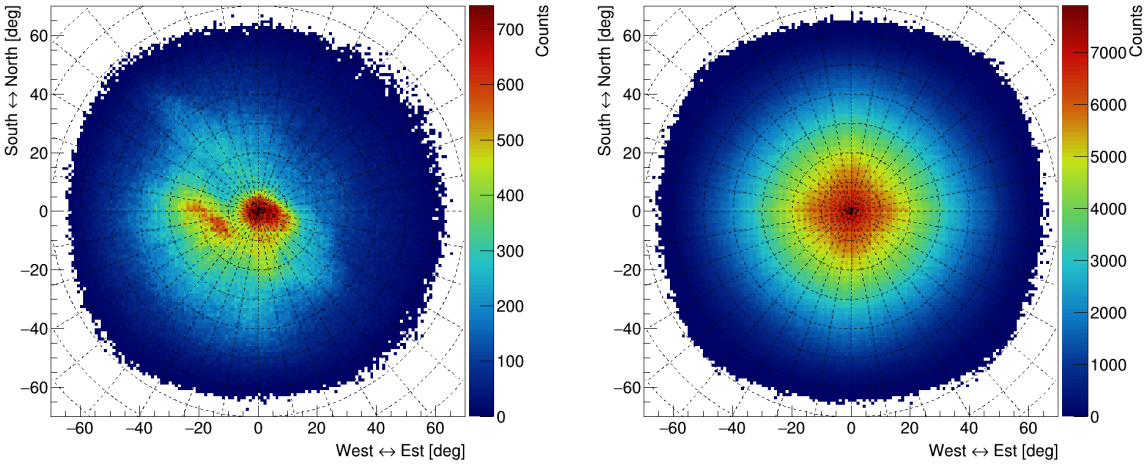

(a) *Target configuration* $N_{tar}(\theta, \varphi)$. **(b)** *Free sky configuration* $N_{free}(\theta, \varphi)$.

Figure 4. Track angular distribution $N(\theta, \varphi)$ for the two different configurations. All the maps are reported using the polar reference frame: in the center there is the vertical direction, the circles correspond to directions with the same zenith angle θ and the lines indicate directions with the same azimuth angle φ (both are represented with a 10° step).

where θ is the angle between the line of sight and the vertical direction, called zenith angle, φ is the pointing angle from the North direction, known as azimuth angle, $\Phi_{\mathrm{M,tar}}$ is the muon flux reaching the detector inside the mine (in the target configuration) and $\Phi_{\mathrm{M,free}}$ is the measured flux in the free sky configuration.

The measured flux in each configuration can be computed as:

$$\Phi_{\mathrm{M}}(\theta, \varphi) = \frac{N(\theta, \varphi)}{t\, A_{\mathrm{eff}}(\theta, \varphi)}$$

where $N(\theta, \varphi)$ is the number of detected tracks with direction (θ, φ), t is the acquisition time and $A_{\mathrm{eff}}(\theta, \varphi)$ is the effective area of the detector for that direction taking into account all the efficiency factors including the efficiency of the analysis.

The angular distributions of the number of reconstructed tracks $N(\theta, \varphi)$ are reported in Figure 4 for the two different configurations. For these and all the following maps we have not used the standard zenithal reference frame but we have used a polar reference frame where the distance from the center of the map represents the zenith angle θ (the center corresponds to the vertical direction) and the azimuth angle φ is the angle from the North direction that is pointing upwards in the maps. In this way it is easier to compare this kind of maps with the cartographic ones.

Supposing that $A_{\mathrm{eff}}(\theta, \varphi)$ remains the same in the two configurations and their relative analysis we obtain that:

$$T_{\mathrm{M}}(\theta, \varphi) = \frac{N_{\mathrm{tar}}(\theta, \varphi)}{N_{\mathrm{free}}(\theta, \varphi)} \frac{t_{\mathrm{free}}}{t_{\mathrm{tar}}}.$$

In Figure 5.a we report the measured transmission in the polar reference frame. To reduce the statistical fluctuations and enhance the correlation between adjacent bins a smoothing filter was used.

Hence the measured transmission can be compared to the expected value. From the digital terrain model of the area we can create a map of the rock depth along the line of sight of the detector for each direction $L(\theta, \varphi)$ assuming the absence of any cavity. A single muon radiography can infer information regarding the amount of matter, or opacity X traversed by the particle along a certain direction that is defined as:

Preprints (www.preprints.org) | NOT PEER-REVIEWED | Posted: 26 November 2018 doi:10.20944/preprints201811.0595.v1

Peer-reviewed version available at Universe 2019, 5, 34; doi:10.3390/universe5010034

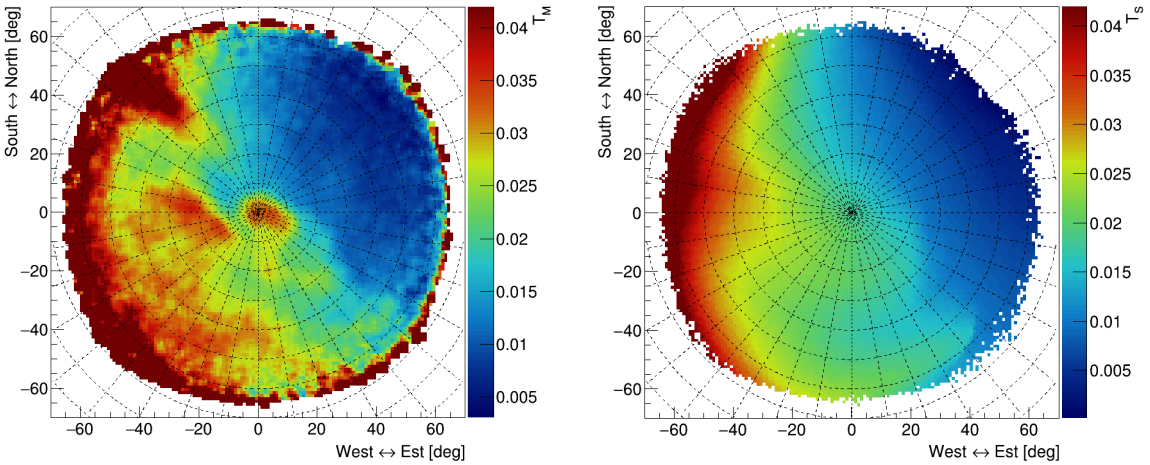

(a) *Measured transmission* T_M. **(b)** *Simulated transmission* T_S.

Figure 5. Measured and simulated muon transmission in the polar reference frame. For the measured transmission a smoothing algorithm was used to reduce the statistical fluctuations and enhance the correlation between adjacent bins. For the simulated transmission we have chosen $\bar{\rho}(\theta, \varphi) = 3$ g cm^{-3}.

$$X(\theta, \varphi, \bar{\rho}) = \int_{\text{l.o.s.}} \rho \, dL = \bar{\rho}(\theta, \varphi) \, L(\theta, \varphi)$$

where ρ is the density of the traversed matter, the integral is computed along the line of sight (l.o.s.) defined by the direction (θ, φ) and $\bar{\rho}$ is the average density in that direction. The opacity X is strictly related to the simulated transmission T_S that can be defined as in formula 1 but this time we have to use the simulated fluxes for the two configurations. The simulated fluxes can be computed as:

$$\Phi_{\text{S,tar}}(\theta, \varphi, \bar{\rho}) = \int_{E_{\min}(X)}^{\infty} \phi(\theta, \varphi, E) \, dE$$
$$\Phi_{\text{S,free}}(\theta, \varphi) = \int_{E_0}^{\infty} \phi(\theta, \varphi, E) \, dE$$

where $\phi(\theta, \varphi, E)$ is the differential muon flux as a function of both the muon energy E and the muon incoming direction (θ, φ), $E_{\min}(X)$ is the minimum energy that muons must have in order to cross the opacity X and reach the detector in the target configuration and E_0 is the minimum energy required to detect muons in the free sky configuration, estimated at about 130 MeV, because of the opacity of the detector itself. For the differential muon flux $\phi(\theta, \varphi, E)$ we have chosen to use the one measured by the ADAMO experiment [18].

The simulated transmission in the polar reference frame is reported in Figure 5.b assuming for the average density $\bar{\rho}(\theta, \varphi)$ a constant value of 3 g cm^{-3}.

The presence of a cavity is thus identified by an excess in the measured transmission relative to the simulated one. The relative transmission, defined as $R(\theta, \varphi, \bar{\rho}) = T_{\text{M}}(\theta, \varphi) / T_{\text{S}}(\theta, \varphi, \bar{\rho})$, will be roughly equal to one in case the correct average rock density is chosen but it will be greater than one when the average density for a certain line of sight is lower than the one used for the simulation (this could be related to the presence of a cavity) and less than one when the average density is higher.

A map of the relative transmission in the polar reference frame obtained for a constant average density of 3 g cm^{-3} is reported in Figure 6.a. From the map we can observe a perfect overlap between the signal region in the North-West direction and the position of the first part of the Gran Cava, marked with black points, where the cave is higher. The large signal in the center of the map corresponds to the Gran Cava end where there is a vertical opening that was not reported in the digital terrain model.

Preprints (www.preprints.org) | NOT PEER-REVIEWED | Posted: 26 November 2018 doi:10.20944/preprints201811.0595.v1

Peer-reviewed version available at Universe 2019, 5, 34; doi:10.3390/universe5010034

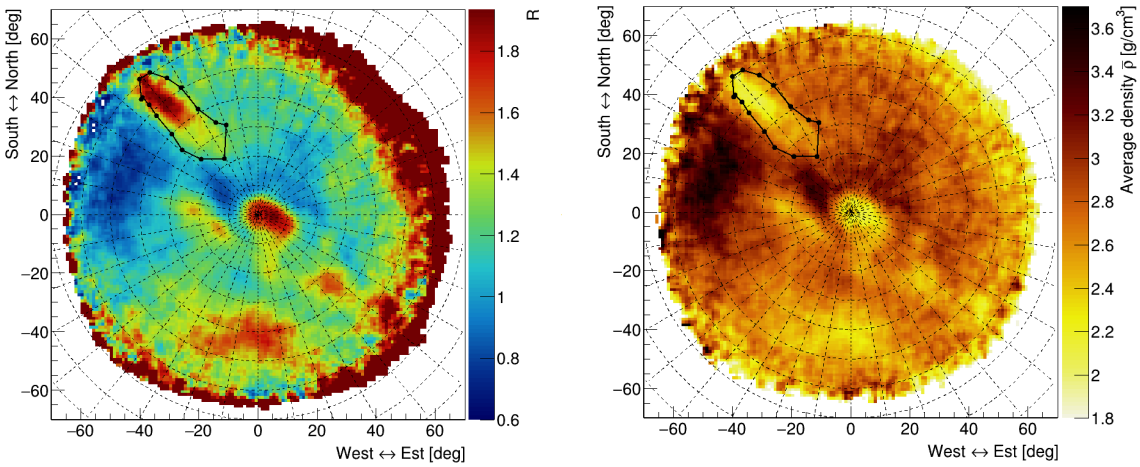

(a) *Relative transmission R.* **(b)** *Average density $\bar{\rho}$.*

Figure 6. Relative transmission and average density maps in the polar reference frame with smoothing filter. The first part of the Gran Cava is marked with black points. We can observe the similarity with the dark area of Figure 3.a thanks to the choice of the polar reference frame.

Consequently this opening, not having been taken into account in the simulation, is revealed as a void. From the Gran Cava position (see Figure 3.a) we would expect a continuity between these two signal regions that is missing. This fact can be due to the presence of a high density rock mass caused by the high concentration of sulfides. In this way the high density rock volume could compensate the effect of the overlying cavity by removing the continuity. This hypothesis is supported by the presence of low relative transmission area (in blue) along the West-Est direction crossing the Gran Cava region. We have also obtained other signal regions that could correspond to unknown cavities. However conclusive statements cannot be made because of the coarseness of the digital terrain model of the overlying hill: for this first analysis we have used an interpolation of a model with a spatial resolution of 10 meters. The red region near the boundary of the acceptance is not particularly relevant because of the low statistics and the uncertainty on the digital terrain model.

Changing the density value for each direction in order to normalize to one the relative transmission we can obtain the average density distribution $\bar{\rho}$ as a function of the direction (θ, φ) as reported in Figure 6.b. The obtained density values are compatible with those of the rocks actually present in the mine.

5. Results and developments

The MIMA detector was installed in a gallery in the Temperino mine in Campiglia Marittima, and took data in a 53 days run. The muography technique was used to identify the Gran Cava. Hints of the existence of so far unknown cavities and of a high density rock vein have been obtained. More precise simulation analysis are ongoing both to increase the digital terrain model precision and to take into account the known accessible cavity. Further measurements will be performed from different locations, in order to triangulate the observed cavities and obtain an estimate of their positions. For the development of the simulation we would try to integrate a voxelization of the inspected volume setting a variable density for every voxel. This would permit us to take into account the presence of known cavities and higher density regions.

Author Contributions: Conceptualization, L.B., V.C., A.D. and R.D.; methodology, L.B. and P.N.; software, G.B., L.B., M.B., V.C., N.M. and L.V.; formal analysis, G.B., L.B., S.Gonzi, L.L.; investigation and installation, G.B., L.B., M.B., R.C., V.C., A.D., C.D., R.D., G.G., S.Gonzi, L.L., B.M., M.N. and L.V. ; resources, D.B., L.C., S.Guideri, G.S.; data curation, G.B., L.B., S.Gonzi, L.L. and B.M.; writing—original draft preparation, G.B.; writing—review and

editing, all authors; visualization, G.B., L.B. and L.L.; supervision and project administration, L.B., D.B., N.C. and R.D..

Funding: The development of the MIMA tracker was funded by INFN and by the Department of Physics and Astronomy of the University of Florence. The travel expenses were funded by the University of Florence and by INFN.

Conflicts of Interest: The authors declare no conflict of interest.

Abbreviations

The following abbreviations are used in this manuscript:

MIMA	Muon Imaging for Mining and Archaeology
MURAVES	MUon RAdiography of VESuvius
INGV	National Institute of Geophysics and Volcanology
INFN	National Institute of Nuclear Physics
SiPM	Silicon PhotoMultiplier
ASIC	Application Specific Integrated Circuit
SDHC	Secure Digital High Capacity
tar	target configuration
free	free sky configuration
l.o.s.	line of sight

References

1. Patrignani, C.; Group, P.D.; others. Review of particle physics. *Chinese physics C* **2016**, *40*, 100001.
2. George, E. Cosmic rays measure overburden of tunnel. *Commonwealth Engineer* **1955**, *455*.
3. Alvarez, L.W.; Anderson, J.A.; El Bedwei, F.; Burkhard, J.; Fakhry, A.; Girgis, A.; Goneid, A.; Hassan, F.; Iverson, D.; Lynch, G.; others. Search for hidden chambers in the pyramids. *Science* **1970**, *167*, 832–839.
4. Tanaka, H.; Nagamine, K.; Kawamura, N.; Nakamura, S.; Ishida, K.; Shimomura, K. Development of a two-fold segmented detection system for near horizontally cosmic-ray muons to probe the internal structure of a volcano. *Nuclear Instruments and Methods in Physics Research Section A: Accelerators, Spectrometers, Detectors and Associated Equipment* **2003**, *507*, 657–669.
5. Anastasio, A.; Ambrosino, F.; Basta, D.; Bonechi, L.; Brianzi, M.; Bross, A.; Callier, S.; Cassese, F.; Castellini, G.; Ciaranfi, R.; others. The MU-RAY experiment. An application of SiPM technology to the understanding of volcanic phenomena. *Nuclear Instruments and Methods in Physics Research Section A: Accelerators, Spectrometers, Detectors and Associated Equipment* **2013**, *718*, 134–137.
6. Carloganu, C.; Tomuvol Collaboration. Density Imaging of Volcanoes With Atmospheric Muons using GRPCs. Proceedings of the XXIst International Europhysics Conference on High Energy Physics (EPS-HEP2011). 21-27 July 2011. Grenoble, 2011, p. 55.
7. Jourde, K.; Gibert, D.; Marteau, J.; de Bremond D'Ars, J.; Komorowski, J.C. Muon dynamic radiography of density changes induced by hydrothermal activity at the La Soufrière of Guadeloupe volcano. *Scientific Reports* **2016**, *6*, 33406. doi:10.1038/srep33406.
8. Schouten, D.; Ledru, P. Muon Tomography Applied to a Dense Uranium Deposit at the McArthur River Mine. *Journal of Geophysical Research: Solid Earth* **Accepted Article**.
9. Saracino, G.; Amato, L.; Ambrosino, F.; Antonucci, G.; Bonechi, L.; Cimmino, L.; Consiglio, L.; D'Alessandro, R.; De Luzio, E.; Minin, G.; Noli, P.; Scognamiglio, L.; Strolin, P.; Varriale, A. Imaging of underground cavities with cosmic-ray muons from observations at Mt. Echia (Naples). *Scientific Reports* **2017**, *7*, 1181. doi:10.1038/s41598-017-01277-3.
10. Morishima, K.; Kuno, M.; Nishio, A.; Kitagawa, N.; Manabe, Y.; Moto, M.; Takasaki, F.; Fujii, H.; Satoh, K.; Kodama, H.; others. Discovery of a big void in Khufu's Pyramid by observation of cosmic-ray muons. *Nature* **2017**, *552*, 386–390.
11. Guardincerri, E.; Rowe, C.; Schultz-Fellenz, E.; Roy, M.; George, N.; Morris, C.; Bacon, J.; Durham, M.; Morley, D.; Plaud-Ramos, K.; Poulson, D.; Baker, D.; Bonneville, A.; Kouzes, R. 3D Cosmic Ray Muon Tomography from an Underground Tunnel. *Pure and Applied Geophysics* **2017**, *174*, 2133–2141. doi:10.1007/s00024-017-1526-x.

12. Saracino, G.; Ambrosino, F.; Bonechi, L.; Bross, A.; Cimmino, L.; Ciaranfi, R.; D'Alessandro, R.; Giudicepietro, F.; Macedonio, G.; Martini, M.; others. The MURAVES muon telescope: technology and expected performances. *Annals of Geophysics* **2017**, *60*, 0103.
13. Morishima, K.; Kuno, M.; Nishio, A.; Kitagawa, N.; Manabe, Y.; Moto, M.; Takasaki, F.; Fujii, H.; Satoh, K.; Kodama, H.; Hayashi, K.; Odaka, S.; Procureur, S.; Attié, D.; Bouteille, S.; Calvet, D.; Filosa, C.; Magnier, P.; Mandjavidze, I.; Riallot, M.; Marini, B.; Gable, P.; Date, Y.; Sugiura, M.; Elshayeb, Y.; Elnady, T.; Ezzy, M.; Guerriero, E.; Steiger, V.; Serikoff, N.; Mouret, J.B.; Charlès, B.; Helal, H.; Tayoubi, M. Discovery of a big void in Khufu's Pyramid by observation of cosmic-ray muons. *Nature* **2017**, *552*, 386–390. doi:10.1038/nature24647.
14. Bonechi, L.; Ambrosino, F.; Cimmino, L.; D'Alessandro, R.; Macedonio, G.; Melon, B.; Mori, N.; Noli, P.; Saracino, G.; Strolin, P.; others. The MURAVES project and other parallel activities on muon absorption radiography. EPJ Web of Conferences. EDP Sciences, 2018, Vol. 182, p. 02015.
15. Baccani, G.; Bonechi, L.; Ciaranfi, R.; Cimmino, L.; Ciulli, V.; D'Alessandro, R.; Melon, B.; Noli, P.; Saracino, G.; Viliani, L. The MIMA project. Design, construction and performances of a compact hodoscope for muon radiography applications in the context of Archaeology and geophysical prospections. *arXiv preprint arXiv:1806.11398* **2018**.
16. Vezzoni, S.; Dini, A.; Rocchi, S. Reverse telescoping in a distal skarn system (Campiglia Marittima, Italy). *Ore Geology Reviews* **2016**, *77*, 176–193.
17. Dini, A.; Guideri, S.; Orlandi, P. *Miniere e minerali del Campigliese - Il mondo sotterraneo del Parco di San Silvestro*; Gruppo Mineralogico Lombardo, Milano (ITA), 2013; p. 98.
18. Bonechi, L.; Bongi, M.; Fedele, D.; Grandi, M.; Ricciarini, S.; Vannuccini, E. Development of the ADAMO detector: test with cosmic rays at different zenith angles. *International Cosmic Ray Conference* **2005**, *9*, 283.